Quantative Susceptibility Mapping: Pulse Sequence Considerations

Wei Li, Chunlei Liu
Brain Imaging & Analysis Center
Duke University
Durham NC 27705, USA

Bing Wu
GE Healthcare
Beijing 100071, China

***Abstract*—the development of fast 3D gradient echo (GRE) sequence and the comprehensive understanding of the dependence of phase and susceptibility contrasts on sequence parameters are important for routine applications of quantitative susceptibility mapping (QSM) and susceptibility tensor imaging (STI). In this study, we developed several GRE sequences for QSM and STI, including different versions of multi-echo SPGR, EPI and Spiral sequences. With appropriate acquisition parameters, these pulse sequences offer a spectrum of choices for various research and clinical applications. We compared the proposed sequences in terms of spatial resolution, scan time, success rates and a few other parameters that are important for selecting the optimal pulse sequence. We also investigated the dependence of phase/susceptibility contrast on different sequence parameters, including slice thickness, TE, TR and flip angle. While phase and susceptibility are independent of slice thickness, both of them are dependent on TE, TR and flip angle. These results demonstrate that both the selection of appropriate pulse sequence and the choice of optimal sequence parameters are important for the application of QSM.**

Keywords—Quantative susceptibility mapping; pulse sequence; phase and susceptibility contrast.

I. INTRODUCTION

Recently, the development of QSM and STI has created many exciting novel opportunities for studying the human brain [1-8]. QSM and STI have demonstrated many advantages in depicting the brain anatomical details [9, 10], in assessing the molecular and cellular components with different magnetic properties from bulk water, particularly myelin and iron [5, 11, 12], and for probing the white matter fiber architectures [6, 8, 13-15]. Furthermore, they have found promising applications in many neurological diseases, e.g. cerebral microbleeds [16], Parkinson's diseases [17], multiple sclerosis [18] and etc. However, one challenge for routine application of QSM and STI is the lengthy scan time due to the requirement of a 3D scan, the long TE needed to accumulate sufficient phase contrast, and sometimes the multi-orientation acquisitions for QSM using COSMOS or for STI. Given the desired time frame, different applications also often have different requirement on the spatial resolution, the signal- or contrast-to-noise ratio (SNR or CNR) and etc. For example, higher spatial resolution is especially desirable for examining the iron content in the small gray matter nuclei, and higher CNR is needed to detect focal lesions in multiple sclerosis. Therefore, the development of fast pulse sequences with a range of options is important to meet the needs of various applications.

This study is supported by NIH through grant ROI1 MH096979 to C.L.

In addition to select the pulse sequence, the choice of sequence parameters is also important. It is well known that the magnitude contrast of GRE signal varies significantly as a function of sequence parameters such as TR, TE and flip angle due to the multi-compartment properties of brain tissues [19]. However, the dependence of phase contrast on these sequence parameters is much less evaluated. Schweser et al first showed that the phase of brain tissue evolves as a nonlinear function of TE [20]. This nonlinear evolution of phase was attributed to local field variation induced by myelin lipids with anisotropic magnetic susceptibility [21, 22]. In addition to TE, we found that TR and flip angle can also affect the phase contrast and its derived magnetic susceptibility due to the differential T1 decays of different tissue micro-compartments [23]. The knowledge of the dependence of phase/susceptibility contrast on these sequence parameters is important not only for developing optimal pulse sequences, but also for comparing results obtained from different studies.

In this study, we will introduced several pulse sequences for QSM and STI that were developed by our group, including different versions of the multi-echo SPGR, EPI and Spiral sequences. We evaluated these pulse sequences in terms of SNR, spatial resolution, scan time, reliability, accuracy and several other parameters that are important for selecting pulse sequences. Finally, we examined the dependence of phase and susceptibility contrasts on different sequence parameters.

II. MATERIALS AND METHODS

A. Pulse Sequences

We developed several pulse sequences for QSM and STI, including the multi-echo SPGR sequence (ME-SPGR), the GRAPPA-accelerated multi-echo SPGR sequence (GRAPPA-SPGR), the multi-echo multi-shot spiral sequence (ME-Spiral), and the multi-echo multi-shot EPI (ME-EPI) sequence. Fig. 1A shows the diagram of the ME-SPGR sequence, which is modified from the single-echo SPGR sequence. We fitted as many bipolar readout gradients as possible during each TR to maximize the scan efficiency. The GRAPPA acceleration was added to the y-phase encoding direction to derive the GRAPPA-SPGR sequence. Fig. 1B&C showed the ME-Spiral sequence [24]. This sequence includes 5 equidistant spiral-out trajectories with a separation of 10ms. A uniform density spiral trajectory consisting of 18 interleaves was used with a 8.4 ms readout duration. Fig. 1D&E shows the ME-EPI sequence. This EPI sequence includes 3 equidistant 16-shot EPI trajectories, in which ramp sampling is used to further increase

the data acquisition efficiency. The phase differences between adjacent even and odd k-space segments with opposite gradient polarities were corrected using additional non-phase encoded reference scans.

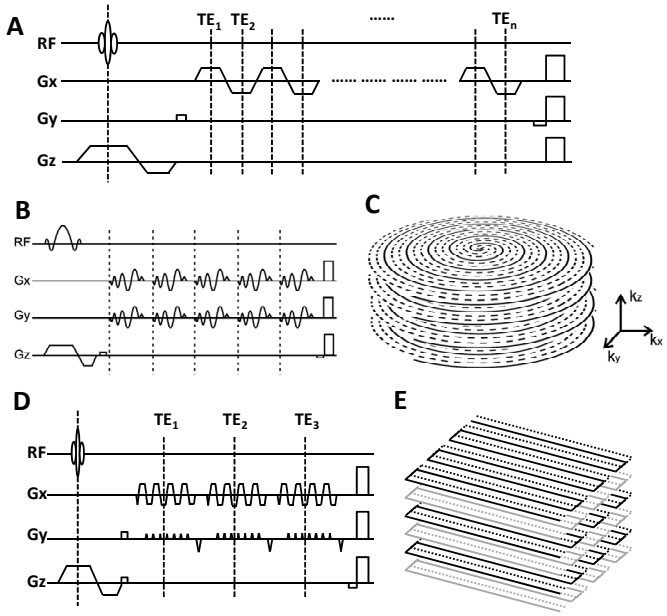

Fig. 1. The diagrams of the ME-SPGR sequence (A), the ME-Spiral sequence (B&C) and the ME-EPI sequence (D&E).

B. Human brain imaging in vivo

We performed several series of experiments to evaluate the developed pulse sequences:

(1) Anisotropic spatial resolution with thick slice is often used to reduce scan time and to compensate for the SNR loss due to the use of fast imaging methods. We scanned 5 healthy subjects with 1mm isotropic resolution using the MR-SPGR sequence. The through-plane resolution was down-sampled to evaluate the impact of thick slice on the accuracy of QSM.

(2) While the ME-Spiral has been compared with the standard SPGR sequence in detail [24], we compared the ME-EPI with the standard SPGR sequence in this study. The parameters for ME-EPI were: field of view (FOV) = 22cm, flip angle = 20º, TE1 = 15ms, 3 echoes, echo spacing = 21ms, TR = 88 ms, slice thickness = 2mm, matrix size = 256x256, and in-plane resolution=0.86x0.86 mm^2, 2 averages. The parameters for SPGR were TE1=4 ms, 16 echoes, echo spacing = 2.56 ms, TR = 56ms, 1 scan average.

(3) We have optimized several versions of the pulse sequences for different applications. Here we compared them in terms of scan time, spatial resolution, SNR, success rates, and several other parameters that are important for the selections of pulse sequences. The comparisons were made using existing data that were acquired in our center.

(4) We evaluated the dependence of phase contrast between gray and white matter on TE, TR and flip angle using the ME-SPGR sequence. Two datasets were acquired. The first dataset has multiple flip angles with the following parameters: flip angle = 5º, 20º, 40º and 60º; TE1=4 ms, echo spacing = 2.12 ms, TR = 50 ms, voxel size = 1x1x2 mm^3. The second dataset has multiple TRs with the following parameters: flip angle = 30º; TE1=4 ms, echo spacing = 2.12 ms, TR = 46 ms, 150 ms and 1s, voxel size = 1x1x3 mm^3.

C. Image analysis

The images were reconstructed using standard methods for Cartesian, spiral and EPI trajectories. The GRE signal phase for each coil was unwrapped using the Laplacian-based phase unwrapping [11]. The phase differences between different coils were removed and the resulting phase was combined with the magnitude to yield the complex image. The combined phase was calculated from combined complex data and then unwrapped. The background phase were removed using a modified SHARP method [25] with decreasing spherical mean filter size towards the brain boundary [11]. The susceptibility maps were derived using the LSQR method [11].

To describe the signal variations of gray-white matter phase contrast as a function of TE, TR and flip angle, we developed a two-compartment model [23]. We assume that gray matter has a single compartment with a constant frequency, while white matter has two compartments, i.e. the myelin water and other water, with different frequencies. The complex MR signals can then be derived as:

$$S(TE)=\sum_{i=1}^{n}\rho_i \exp\left(j\cdot 2\pi\Delta f_i t-\frac{TE}{T_{2,i}^*}\right)\cdot\sin\theta\cdot\frac{1-\exp\left(-TR/T_{1,i}\right)}{1-\exp\left(-TR/T_{1,i}\right)\cos\theta} \quad [1]$$

Where S is total NMR signal, ρ is the relative pool size of the compartment, f is the frequency shift of each compartment using the gray matter frequency as the reference, and θ is the flip angle. The parameters can be obtained by fitting the magnitude and frequency shift of white matter with multiple TR or flip angles. This model have 7 parameters. To improve the data fitting stability, we used a fixed myelin water fraction of 13%, according a previous study [26].

III. Results

A. The accuracy of QSM is independent of slice thickness

Fig. 2A compares the magnetic susceptibility maps obtained with different slice thicknesses. Despite the complicated susceptibility mapping steps, their difference is

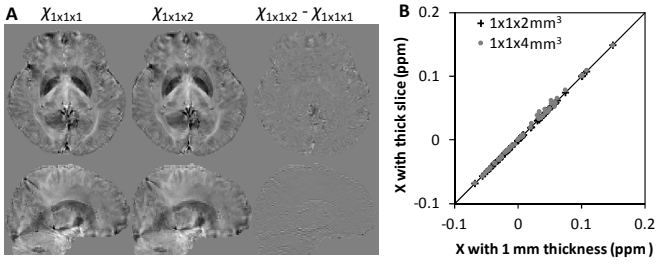

Fig. 2. Dependence of QSM results on slice thickness. A: susceptibility maps with different slice thickness and their differece image. B: Plot of susceptibility value of low through-plane resolution against that obtained from original spatial resolution.

small, and limited to tissue boundaries. We plotted the susceptibility values of the selected anatomical structures using the lower through-plane resolution images against that using original image with 1mm isotropic resolution. The error due to slice thickness is negligible comparing to the physiological variations of magnetic susceptibility across different brain regions. These results show that it is valid to use thick slice for QSM.

B. Phase and susceptibility contrast by different sequences

Previously, Wu et al showed that the susceptibility contrast by ME-Spiral was very similar to that of SPGR, and the susceptibility values of different nuclei is also similar to that of SPGR quantitatively [24], as shown in Table I.

TABLE I. COMPARISON OF MAGNETIC SUSCEPTIBILITY VALUES USING THE ME-SPIRAL AND THE STANDARD SPGR SEQUENCE [24]

$\chi\pm\Delta$ × (0.01ppm)	*PU*	*SN*	*RN*	*GP*
Spiral	4.3 ± 0.6	4.3 ± 0.6	6.1 ± 0.4	9.4 ± 1.1
SPGR	4.7 ± 0.4	4.7 ± 0.4	6.2 ± 0.5	9.0 ± 1.0

Here we compared with the results of ME-EPI with that of magnetic susceptibility. Fig. 3 shows that the frequency shifts and magnetic susceptibility determined by ME-EPI and SPGR were very similar.

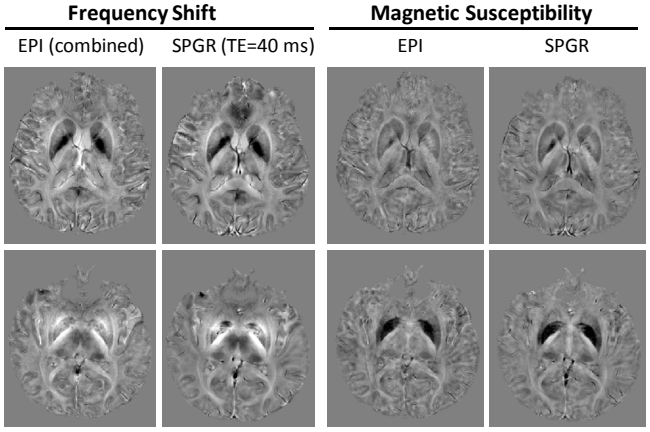

Fig. 3. Comparision of frequency shifts and magneic susceptibility maps by ME-EPI and SPGR.

Quantitatively, the susceptibility values of selected gray matter regions were also similar to that of SPGR (Fig. 4). These results demonstrated the validity of using ME-Spiral or ME-EPI for QSM and STI applications.

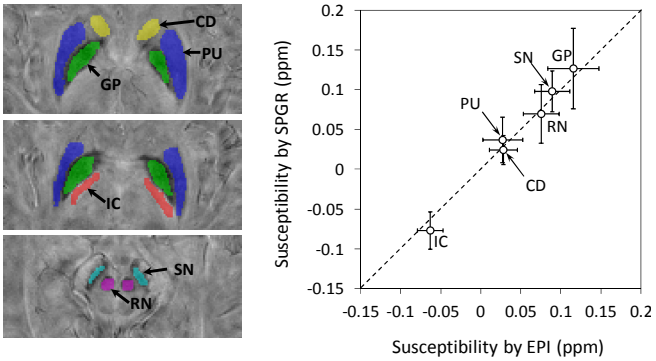

Fig. 4. Comparision of magnetic susceptibility values by ME-EPI and SPGR.

C. The comparision of different pulse squences

By selecting appropriate acquisition parameters, the above pulse sequences can provide a variety of options to meet the needs of different research and clinical applications. We summarized a comparison of these pulse sequences in several of our successful applications in Table II. All these sequences were intended for covering the whole brain with sufficient SNR and spatial resolution. In general, given sufficient scan time of 6 min or more, the GRAPPA-SPGR sequence provides excellent image quality and success rates. For applications with less available time, ME-Spiral and ME-EPI provide viable choices. While ME-Spiral provides higher SNR, it has less success rates due to susceptibility induced blurring artifacts. ME-EPI has slightly less SNR, but offers higher success rates.

D. Dependence of phase contrast on squence parameters

Fig. 4 showed that the gray-white matter phase contrast is dependent on TE, TR and flip angle. This dependence can be fitted by the two-compartment model as described by Eq. [1].

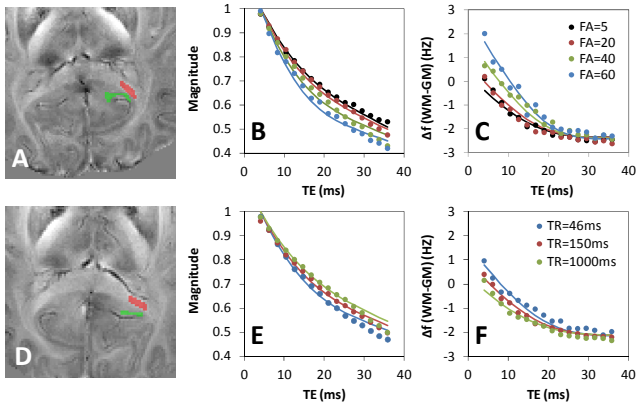

Fig. 4. The dependence of magnitude and phase of white matter on scan parameters. The gray matter is used as the reference for white matter.

TABLE II. CPMPARISION OF DIFFERENT PULSE SEQUENCES

	# of echoes	*TR (ms)*	*Matrix size*	*# of slices*	*Voxel size (mm^3)*	*Scan time (min)*	*SNR of χ*	*Success rate*
ME-SPGR (40ms)	16	55	192x192	120	1x1x1	21.2	74	>95% (n=40)
GRAPPA-SPGR	10	41	288x254	54	0.8x0.8x2	5.8	55	90% (n=10)
ME-SPIRAL	5	70	192x192	120	1x1x1	2.5	44	62% (n=8)
ME-EPI (NEX=2)	3	88	256x256	64	0.9x0.9x2	3.0	39	75% (n=8)
ME-EPI (NEX=1)	3	88	256x256	64	0.9x0.9x2	1.5	28	-

The fitted parameters were summarized in Table III. In general, the phase contrast between gray and matter approaches to similar contrast after 20~30ms.

TABLE III. PARAMETERS FOR THE TWO-COMPARTMENT MODEL

	Myelin water		**Other water**	
	Multi-FA	***Multi-TR***	***Multi-FA***	***Multi-TR***
Δf (Hz)	16.9	15.2	-2.3	-2.1
T2* (ms)	11	12	55	65
T1 (ms)	72	398	278	969

IV. DISCUSSION

We have developed several fast multi-echo GRE sequences, including the ME-SPGR, GRAPPA-SPGR, ME-Spiral and ME-EPI sequences. With appropriate parameters, these sequences provide a variety of choices for various QSM and STI applications. Since the accuracy of QSM is independent of slice thickness (Fig. 2), it is often advantageous to use anisotropic voxel size. The higher in-plane resolution can allow clearer delineation of the anatomical details, whereas the thick-slice can reduce the scan time and to compensate for the SNR loss due to the use of fast imaging methods. As such, we often choose a slice thickness of 2 with in-plane resolution of 1 mm or higher in our applications (Table II).

Given enough scan time of 6 min or more, it is usually safe to choose the GRAPPA-SPGR sequence. To further accelerating the scan, either ME-Spiral or ME-EPI sequences can be used. The ME-Spiral sequence allows for fast scan with 1 mm isotropic resolution within 2.5 min, with similar SNR comparing to that of SPGR sequence [24]. However, it is more often affected by susceptibility-induced artifacts. In contrast, the ME-EPI sequence offers more robustness, but with slightly lower SNR. It can provide phase and susceptibility maps with a spatial resolution of 0.86x0.86x2 mm^3 within 3 min, which includes 2 averages. A single average with 1.5 min scan time also gives reasonably well quality for applications that are targeted to medium to large brain structures. The magnetic susceptibility maps derived from ME-Spiral and ME-EPI are in good agreement with that of standard SPGR sequence given the sequence parameters specified in this study.

It is important that the gray-white matter phase contrast is dependent on TR, TE and flip angles. Therefore, it is critical to keep the same TR, TE and flip angles throughout a given application of QSM. On the other hand, this signal variation may also offer an exciting possibility to sensitize the phase/susceptibility contrast to specific diseased conditions by simply manipulating the sequence parameters.

REFERENCES

[1] C. Liu, "Susceptibility tensor imaging," *Magn. Reson. Med.,* vol. 63, pp. 1471-1477, 2010.

[2] T. Liu, *et al.*, "Calculation of susceptibility through multiple orientation sampling (COSMOS): A method for conditioning the inverse problem from measured magnetic field map to susceptibility source image in MRI," *Magn. Reson. Med.,* vol. 61, pp. 196-204, 2009.

[3] L. de Rochefort, *et al.*, "Quantitative susceptibility map reconstruction from MR phase data using Bayesian regularization: validation and application to brain imaging," *Mag. Reson. Med.,* vol. 63, pp. 194-206, 2010.

[4] S. Wharton, *et al.*, "Susceptibility mapping in the human brain using threshold-based k-space division," *Magn. Reson. Med.,* vol. 63, pp. 1292-1304, 2010.

[5] F. Schweser, *et al.*, "Quantitative imaging of intrinsic magnetic tissue properties using MRI signal phase: An approach to in vivo brain iron metabolism?," *Neuroimage,* vol. 54, pp. 2789-807, 2011.

[6] W. Li, *et al.*, "Magnetic susceptibility anisotropy of human brain in vivo and its molecular underpinnings," *Neuroimage,* vol. 59, pp. 2088-97, 2012.

[7] C. Liu, *et al.*, "Probing white-matter microstructure with higher-order diffusion tensors and susceptibility tensor MRI," *Frontiers in Integrative Neuroscience,* vol. 7, p. 11, 2013.

[8] C. Liu and W. Li, "Imaging neural architecture of the brain based on its multipole magnetic response," *NeuroImage,* 2012.

[9] A. Deistung, *et al.*, "Toward in vivo histology: A comparison of quantitative susceptibility mapping (QSM) with magnitude-, phase-, and R2*-imaging at ultra-high magnetic field strength," *NeuroImage,* vol. 65, pp. 299-314, 2013.

[10] J. H. Duyn, *et al.*, "High-field MRI of brain cortical substructure based on signal phase," *P. Natl. Acad. Sci. USA,* vol. 104, pp. 11796-11801, 2007.

[11] W. Li, *et al.*, "Quantitative susceptibility mapping of human brain reflects spatial variation in tissue composition," *Neuroimage,* vol. 55:1645-1656, 2011.

[12] C. Liu, *et al.*, "High-field (9.4 T) MRI of brain dysmyelination by quantitative mapping of magnetic susceptibility," *Neuroimage,* vol. 56, pp. 930-938, 2011.

[13] C. Liu, *et al.*, "3D Fiber tractography with susceptibility tensor imaging," *Neuroimage,* vol. 59, pp. 1290-1298, 2012.

[14] X. Li, *et al.*, "Mapping magnetic susceptibility anisotropies of white matter in vivo in the human brain at 7T," *NeuroImage,* vol. 62, pp. 314-330, 2012.

[15] C. Wisnieff, *et al.*, "Magnetic susceptibility anisotropy: Cylindrical symmetry from macroscopically ordered anisotropic molecules and accuracy of MRI measurements using few orientations," *NeuroImage,* vol. 70, pp. 363-376, 2013.

[16] T. Liu, *et al.*, "Cerebral microbleeds: burden assessment by using quantitative susceptibility mapping," *Radiology,* vol. 262, pp. 269-278, 2012.

[17] A. K. Lotfipour, *et al.*, "High resolution magnetic susceptibility mapping of the substantia nigra in Parkinson's disease," *Journal of Magnetic Resonance Imaging,* vol. 35, pp. 48-55, 2012.

[18] C. Langkammer, *et al.*, "Quantitative Susceptibility Mapping in Multiple Sclerosis," *Radiology,* 2013.

[19] D. Hwang, *et al.*, "In vivo multi-slice mapping of myelin water content using T2* decay," *NeuroImage,* vol. 52, pp. 198-204, 2010.

[20] F. Schweser, *et al.*, "Non-linear evolution of GRE phase as a means to investigate tissue microstructure," in *Proc Int Soc Magn Reson Med*, 2011.

[21] P. Sati, *et al.*, "Micro-compartment specific T2* relaxation in the brain," *NeuroImage,* vol. 77, pp. 268-278, 2013.

[22] S. Wharton and R. Bowtell, "Fiber orientation-dependent white matter contrast in gradient echo MRI," *Proceedings of the National Academy of Sciences,* vol. 109, pp. 18559-18564, 2012.

[23] W. Li, *et al.*, "Dependence of gradient echo phase contrast on the differential signal decay in subcellular compartments," *Proc Int Soc Magn Reson Med,* vol. 21, 2013.

[24] B. Wu, *et al.*, "Fast and tissue-optimized mapping of magnetic susceptibility and T2* with multi-echo and multi-shot spirals," *Neuroimage,* vol. 59, pp. 297-305, 2012.

[25] F. Schweser, *et al.*, "Quantitative imaging of intrinsic magnetic tissue properties using MRI signal phase: An approach to in vivo brain iron metabolism?," *Neuroimage,* 2010.

[26] D. Hwang, *et al.*, "In vivo multi-slice mapping of myelin water content using T-2* decay," *NeuroImage,* vol. 52, pp. 198-204, 2010.